



The z-spectrum from human blood at 7T

Simon M. Shah^{a,*}, Olivier E. Mougin^a, Andrew J. Carradus^a, Nicolas Geades^a, Richard Dury^a, William Morley^a, Penny A. Gowland^{a,b}

^a Sir Peter Mansfield Imaging Centre, School of Physics and Astronomy, University of Nottingham, Nottingham, UK

^b NIHR Nottingham Biomedical Research Centre, Nottingham University Hospitals NHS Trust, University of Nottingham, Nottingham, UK

ARTICLE INFO

Keywords:

Chemical exchange saturation transfer (CEST)
Nuclear overhauser enhancement (NOE)
Z-spectrum
Magnetisation transfer
Blood relaxometry

ABSTRACT

Chemical Exchange Saturation Transfer (CEST) has been used to assess healthy and pathological tissue in both animals and humans. However, the CEST signal from blood has not been fully assessed. This paper presents the CEST and nuclear Overhauser enhancement (NOE) signals detected in human blood measured via z-spectrum analysis. We assessed the effects of blood oxygenation levels, haematocrit, cell structure and pH upon the z-spectrum in *ex vivo* human blood for different saturation powers at 7T. The data were analysed using Lorentzian difference (LD) model fitting and AREX (to compensate for changes in T_1), which have been successfully used to study CEST effects *in vivo*. Full Bloch-McConnell fitting was also performed to provide an initial estimate of exchange rates and transverse relaxation rates of the various pools. CEST and NOE signals were observed at 3.5 ppm, -1.7 ppm and -3.5 ppm and were found to originate primarily from the red blood cells (RBCs), although the amide proton transfer (APT) CEST effect, and NOEs showed no dependence upon oxygenation levels. Upon lysing, the APT and NOE signals fell significantly. Different pH levels in blood resulted in changes in both the APT and NOE (at -3.5 ppm), which suggests that this NOE signal is in part an exchange relayed process. These results will be important for assessing *in vivo* z-spectra.

Introduction

Z-spectrum features, in particular chemical exchange saturation transfer (CEST) have recently been used to study both healthy and pathological tissues *in vivo* (van Zijl and Yadav, 2011; Zaiss and Bachert, 2013; Liu et al., 2013), but so far there has only been one study of the z-spectrum of blood (Zheng et al., 2014). The z-spectrum provides a means of indirectly studying proton pools that are conventionally invisible to MRI, opening up the possibility of metabolic imaging with MRI (Cai et al., 2012; Walker-Samuel et al., 2013; Rivlin et al., 2013; van Zijl et al., 2007; Haris et al., 2014; Cai et al., 2015).

CEST (Zaiss and Bachert, 2013; Ward et al., 2000; Zhou and van Zijl, 2006) uses the principles of magnetisation transfer (MT) to investigate moieties containing labile protons by applying saturation at their resonant frequency and detecting the subsequent transfer of the saturation to the water pool via chemical exchange. The transferred saturation can only be detected if the chemical exchange is fast compared to the longitudinal recovery rate but in the slow to intermediate regime compared to the chemical shift between the water and the labile protons. Amide proton transfer (APT) CEST is associated with mobile amide protons at

$+3.5$ ppm relative to water. It is sensitive to pH (Zhou et al., 2003) and has been applied to study ischemia and tumour grading, but its origins are not fully understood. The increase in APT in tumours has been attributed to an increase in the content of endogenous cellular proteins and peptides, despite the fact that the total content of proteins has been shown to be relatively constant in tumours (Yan et al., 2015). Amines (NH_2) at 2.2 ppm are in faster exchange than APT, but are infrequently detected *in vivo* since high saturation powers are required. The amine signal has previously been used as a marker for pH (McVicar et al., 2014). The NOE signal at -3.5 ppm was believed to originate from regions of high myelination (Mougin et al., 2013; Jones et al., 2013) however, more recently Xu et al. showed that there is no NOE contrast difference between grey and white matter when the magnetisation transfer contrast is suppressed (Xu et al., 2016). The NOE signal may also be decreased in tumours (Zaiss et al., 2015) but this is probably related to increased water content and requires further investigation. Jones et al. also investigated multiple NOE peaks associated with the macromolecule MRS spectrum (Jones et al., 2013), and Zhang et al. observed a 'new NOE peak around -1.6 ppm' and showed it was reduced in ischemic stroke (Zhang et al., 2016).

* Corresponding author.

E-mail address: simon.shah@nottingham.ac.uk (S.M. Shah).

<https://doi.org/10.1016/j.neuroimage.2017.10.053>

Received 18 August 2017; Accepted 25 October 2017

Available online 27 October 2017

1053-8119/© 2017 The Authors. Published by Elsevier Inc. This is an open access article under the CC BY license (<http://creativecommons.org/licenses/by/4.0/>).

Zheng et al. found that blood has increased CEST contrast relative to some other tissues (Zheng et al., 2014). However they assessed the CEST signal using MT asymmetry (Zhou et al., 2004), which is sensitive to competing effects of NOE (−3.5 ppm) and APT (+3.5 ppm) particularly at high field.

Asymmetry analysis was the original method used to analyse CEST and NOE signals from *in vivo* MRI but recently alternative quantification approaches have been proposed, such as Lorentzian difference (LD) fitting and AREX (Zaiss et al., 2011). LD fitting can characterise slow and intermediate exchanging proton pools but is not suitable for faster exchanging proton pools (such as amines and hydroxyls) which coalesce with the water signal (Zaiss and Bachert, 2013). To directly estimate the absolute sizes of the exchanging pools relative to water it is necessary to fit the data to a multi-pool Bloch-McConnell (BM) model (van Zijl and Yadav, 2011; Chappell et al., 2013; Geades et al., 2017). BM fitting is more time consuming than LD fitting and AREX, requires some *a priori* knowledge of parameters such as T_2 and k_{ex} of each exchanging proton pool, and generally requires larger datasets to be used in the fit.

This work aims to investigate the CEST and NOE signals visible in *ex vivo* blood, considering the effects of oxygenation, haematocrit, cell structure and pH, quantifying the results using AREX and also direct BM fitting to provide initial estimates of the exchange rates and transverse relaxation times of the various pools.

Methods

In vivo human data

With local ethical approval, 2 male subjects aged 31 and 35 were recruited and z-spectra were acquired from the head.

Blood collection and preparation

With local ethical approval, a total of 98 ml of venous blood was taken from 4 healthy male volunteers and was stored in vials containing an anticoagulant (heparin) or allowed to clot. The unclotted samples were then treated in various ways with the number of samples used for each treatment shown in Table 1.

Either 120 ml of nitrogen gas or medical (100%) oxygen was bubbled through the blood to deoxygenate or oxygenate it. To achieve this two syringe needles were pushed through the rubber seal of the vials, one connected to a 60 ml syringe to the relevant gas, and the second to exhaust gas from the vial to prevent pressure rise. A very low gas flow rate was used to prevent foaming (Gardener et al., 2010) and the vials were regularly inverted to ensure good mixing. A blood gas analyzer (i-STAT, Abbott) was used to measure the samples' saturation of oxygen (SO_2), partial pressure of oxygen (PO_2), pH and haematocrit (Hct) levels.

8 ml of unmodulated blood was spun in a centrifuge (15 min at 800 rpm) and the plasma was removed. Two such samples were combined to give a concentrated RBC (cRBC) sample with 40% greater Hct level than whole blood. The remaining 12 ml of blood samples were washed with a phosphate saline buffer to modify the pH to 6.8, 7.0 and 7.4. MR scanning was commenced within one hour of blood collection. At the end of scanning, the blood was frozen and defrosted within a week to lyse the blood cells before repeating the scan. This method of lysis causes cells in the blood to swell and ultimately break as ice crystals form during the freezing process. The cell skeletons were left in the samples during the repeated scanning.

A sample of heparinized water was also scanned.

For MR scanning the vials were placed in a temperature controlled holder. The holder was designed to allow warm water to flow slowly around the samples to keep them at 37 °C (PMT Instruments). The holder was rotated every 4 minutes during scanning to limit blood sedimentation, and could be repositioned after each rotation with a mean displacement of 0.01 ± 0.02 mm in the x-direction and 0.11 ± 0.05 mm in y-direction.

Table 1

The number of blood samples taken during the experiments across the 4 healthy male volunteers.

Type of sample	Number of Samples
Control (4 ml)	4
Oxygenated (4 ml)	4
Deoxygenated (4 ml)	3
Concentrated RBCs (2 × 4ml)	4
Plasma (2 × 4ml)	2
Clotted (5 ml)	2
pH 6.8 (4 ml)	1
pH 7.0 (4 ml)	1
pH 7.4 (4 ml)	1
Total	24

MRI acquisition

All MRI experiments were conducted on a 7T Philips Achieva with a volume transmit RF coil and Nova 32 channel receive coil. Z-spectra were obtained using a saturation-prepared 3D TFE sequence (Mougin et al., 2013) shown in Fig. 1. The pulse sequence involved a train of 40 Gaussian windowed sinc RF pulses with bandwidth 200 Hz and a duty cycle of 50% applied prior to a TFE readout with a low-high radial k-space acquisition scheme.

The pulses were phase cycled and a spoiler gradient was applied at the end of the pulse train to remove residual transverse magnetisation. Further details are given in Table 2.

An additional acquisition was made with a presaturation at 167 ppm, which was assumed not to saturate any exchangeable magnetisation. This data point was used to estimate M_0 for normalisation, since we had previously observed that off-resonance pre-saturation resulted in a small change in the amplitude of the readout pulses.

B_0 and B_1 (AFI (Yarnykh, 2007)) maps were acquired to correct for the field inhomogeneities (allowing no change in transmitter calibration between acquisition of the B_1 map and the z-spectrum). T_1 maps were acquired using an inversion recovery sequence with FOV $224 \times 224 \times 48$ mm³ and voxel size $1.5 \times 1.5 \times 2$ mm³, TI = 150, 200, 300, 400, 500, 600, 700, 800, 1000, 1200, 1500, 1800, 2200, 3000, 3500, 4000, 4500 and 5000 ms, TR/TE = 6.9/3.2 ms and SENSE factor (RL) of 2. T_2^* maps were acquired using a multi-gradient echo (echos = 8) with FOV $256 \times 256 \times 48$ mm³ and voxel size $2 \times 2 \times 2$ mm³. TR/TE = 45/1.35 ms and $\Delta TE = 1.8$ ms.

Data processing

Voxel-wise z-spectra were obtained for each RF saturation power by calculating

$$Z(\Delta\omega) = M_{z,sat}(\Delta\omega)/M_0 \quad (1)$$

at each off-resonance ($\Delta\omega$), with normalisation by the signal M_0 acquired at 50 kHz (167 ppm). The z-spectra were B_0 corrected by interpolating to 0.01 ppm resolution between ± 17 ppm, then shifting the entire spectrum by the difference between the B_0 map and the zero point at 0 ppm, and finally re-sampling back to the original off-resonance frequencies (Zaiss and Bachert, 2013; Zhou et al., 2003).

The B_1 map was used to estimate the actual saturation amplitude at which each z-spectrum from each voxel was acquired. Next the z-spectra for the target B_1 amplitudes of 0.5, 0.9 and 1.3 μT were estimated by using spline interpolation between measured z-spectra up to 1.5 μT , including an additional point at 0 μT (Windschuh et al., 2015).

The T_1 relaxation time was calculated by fitting the inversion recovery data to $M = M_0(1 - \alpha \exp(-TI/T_1))$ where α accounted for incomplete inversion. T_2^* was calculated by fitting the natural log of 8 gradient echoes to a linear decay using a weighted least-squared fitting algorithm, excluding any data that fell below background noise.

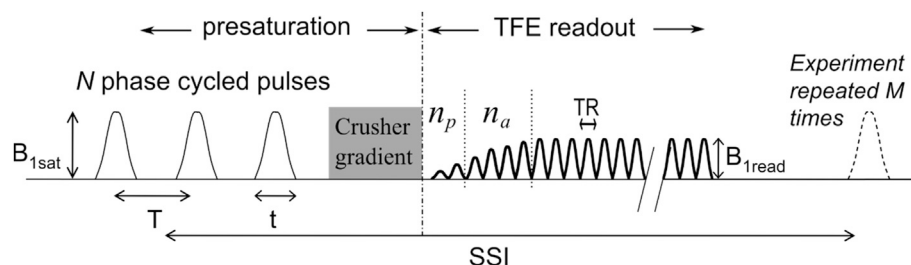


Fig. 1. The magnetisation transfer-prepared turbo field echo (MT-TFE) sequence: a presaturation period followed by the TFE readout. The presaturation period consists of $N = 40$ Gaussian windowed sinc pulse. The duty cycle of 50% was used such that $t = 30$ ms and $T = 60$ ms. The crusher gradient at the end of the saturation train removes any residual transverse magnetisation. $n_p = 2$ and $n_a = 4$ are the number of ramped RF pulses before and at the start of the acquisition, respectively. From (Mougin et al., 2013).

Table 2
MR sequence parameters for the blood samples and *in vivo* acquisition.

	Blood samples	<i>In vivo</i>
$B_{1,max}$ (μ T)	2.4, 4.9 and 8.5	2.4 and 6.0
$B_{1,rms}$ (μ T)	0.43, 0.87 and 1.52	0.43 and 1.1
Off resonance frequencies (ppm)	83 off-resonance frequencies between ± 17 ppm, and at 50 kHz (167 ppm).	38 and 23 off-resonance frequencies between ± 33 ppm, and at 50 kHz (167 ppm) for 2.4 μ T and 6.0 μ T respectively
FOV (mm^3)	$224 \times 224 \times 48$	$192 \times 186 \times 50$
Resolution (mm^3)	$1.5 \times 1.5 \times 2$	$1.5 \times 1.5 \times 1.5$
TE/TR/FA	2.6 ms/5.55 ms/8°	2.8 ms/6 ms/8°
SENSE (RL)	2	2
Number of TFE shots	5	4

To quantify changes in CEST and NOE components, initially Lorentzian difference (LD) model fitting was performed (Zaiss et al., 2011), assuming that the z-spectra could be approximated by a linear combination of Lorentzian functions corresponding to amides (nominally at 3.5 ppm), amines (nominally at 2.2 ppm), the NOEs (nominally at -3.5 and -1.7 ppm), and a Lorentzian corresponding to the MT from macromolecules (Hua et al., 2007; Morrison and Henkelman, 1995). The LD model was fitted to the B_1 corrected z-spectra using a least-square algorithm, allowing the positions of the CEST and NOE peaks to vary by ± 0.4 ppm around the predicted literature values, and the amplitude and width of the peaks to vary. The variations in the position and width of the peaks accounted for the differences in T_2^* and frequency offset between oxygenated and deoxygenated blood.

To account for changes in T_1 , the AREX signal (Zaiss et al., 2015) was calculated,

$$AREX(\Delta\omega) = \left(\frac{1}{Z_{lab}(\Delta\omega)} - \frac{1}{Z_{ref}(\Delta\omega)} \right) / T_1, \quad (2)$$

where T_1 was the observed longitudinal relaxation time, $Z_{lab}(\Delta\omega)$ was the measured Z-value (Equ. 1) at off-resonance frequency $\Delta\omega$ and $Z_{ref}(\Delta\omega)$ was the Z-value from the summation of all fitted Lorentzians, except for the Lorentzian for the proton pool of interest at $\Delta\omega$. Whilst AREX can compensate for changes in T_1 between the fresh and lysed blood samples, it cannot be computed over the total width of the Lorentzian lineshape, and therefore the peak amplitude of the fitted Lorentzian was used. AREX assumes steady state has been achieved and breaks down close to 0 ppm due to the inverse in Equ (2), and therefore it is difficult and sometimes impossible to calculate AREX values for the amines (2.2 ppm) and NOE. 1.7ppm (Heo et al., 2017). Additionally the amine (and other hydroxyls pool) peaks coalesce with the water peak, making them difficult to separate the signals when performing Lorentzian lineshape fitting.

We also fitted the z-spectra acquired at three B_1 saturation powers (162 data points in total) jointly to a 6-pool BM model (Woessner et al., 2005) to provide absolute estimates of the pool sizes $M_{i,0}/M_{f,0}$, T_{i2} , and exchange rate $k_{i,ex}$ of each (*i*th) exchanging proton pool in an iterative manner. These fits were carried out on the University of Nottingham High Performance Computer. The model only allowed for exchange between the off-resonance pools and free water, assuming that direct

exchange between the other pools was negligible. Initially the three spectra from the control blood sample were fitted to the 6-pool model using a genetic algorithm to obtain an initial estimate of the 16 parameters (5 $M_{i,0}/M_{f,0}$, 6 T_{i2} , and 5 $k_{i,ex}$), assuming the water longitudinal relaxation time measured with the inversion recovery experiment, and the RF amplitude from the B_1 map. The starting values for this fit are given in Table 3; these values were taken from brain data (van Zijl et al., 2017) adjusted from preliminary BM fits. We made an estimate of the errors in the fitted parameters by considering the span of possible fitted parameter values consistent with doubling in the sum of squares at the fitted value (which would correspond to halving the signal to noise ratio (SNR) in the spectra if the error in the fit were purely due to random noise).

Next these results were used to estimate the pool sizes $M_{i,0}/M_{f,0}$ for the fresh and lysed control and concentrated samples, assuming no change in T_{i2} , and $k_{i,ex}$. This approach allowed better comparison of the relative pool sizes than if T_{i2} , and $k_{i,ex}$ had been allowed to vary freely. The data from each sample were fitted for 5 parameter to the 6-pool model. For each sample the T_2 of water was estimated from the linewidth of the direct saturation (DS) peak within 400 Hz of resonance.

Results

In vivo APT and amine maps from one volunteer produced by LD fitting are shown in Fig. 2(a–b). Fig. 2(c–d) show the z-spectra and AREX spectra for the regions of interest indicated in Fig. 2(a). Both spectra suggest high APT and amine signals and low NOE signals in the sagittal sinus compared to white matter and grey matter. Similar results were obtained in the other volunteer. Fig. 2(c) shows that the MT asymmetry

Table 3
Starting parameters used for the 6 pool Bloch-McConnell fitting of the z-spectra acquired on the control blood sample for B_1 saturation powers of 0.43, 0.87 and 1.52 μ T.

	APT	Amines	NOE. 1.7ppm	NOE. -3.5ppm	MT
T_2 (ms)	0.5	10	1.2	0.5	0.01
Exchange rate (Hz)	20	500	1.5	5	15
Assumed frequency offset from water (ppm)	3.5	2.2	-1.7	-3.5	-2.34
Assumed T_1 (ms)	1000	1000	1000	1000	1000

observed in WM and GM is not present in blood.

Fig. 3 shows the (a) oxygen saturation (SO_2), partial pressure of oxygen (PO_2), haematocrit, pH and (b) average T_1 and T_2^* , of each set of samples. For all oxygenated samples the SO_2 reached 100% after preparation and maintained this level for the duration of the experiment. The SO_2 of the deoxygenated and control blood was approximately 40% and 80% respectively. Both samples' oxygenation levels changed during the experiment (control SO_2 increased and deoxygenated SO_2 decreased) because the gas in the space above the blood in the vials continued to exchange with the red blood cells. The oxygenated and deoxygenated blood had a PO_2 of approximately 60 and 3 mmHg respectively. The pH levels for all the samples were between 7.3 and 7.5 during scanning, with a drop of pH 0.2–0.3 detected over the course of scanning. The Hct was approximately 40% for the control, oxygenated and deoxygenated blood, over 70% for the concentrated RBCs and less than 10% for plasma.

Fig. 3(b) shows that the T_2^* of the deoxygenated blood was approximately five times shorter than that of the oxygenated and control blood samples. The concentrated RBCs had a shorter T_2^* than the oxygenated and control blood (and also a somewhat lower SO_2), and the plasma had a much longer T_2^* than all the other samples. Lysing the blood shortened the T_1 and lengthened T_2^* for all the blood samples.

The z-spectrum of heparinized water only showed the DS peak.

Figure 4(a) shows B_1 corrected example z-spectra for concentrated RBCs and plasma, including an inset of the AREX spectra. The longer T_2^* of plasma gave a narrower lineshape around 0 ppm, but these spectra indicate that the largest source of the MT, CEST and NOE signal in the blood is from the RBCs rather than plasma. Fig. 4(b) shows no significant

difference in NOE and CEST peaks between the z-spectra for oxygenated and deoxygenated blood. The wider DS peak of the deoxygenated blood is expected due to its shorter T_2^* (Table 4). Fig. 4(b) inset shows the AREX spectra, further suggesting that there no significant difference in the NOE and CEST peaks between the oxygenated and deoxygenated spectra.

Fig. 4(b) and (c) suggest considerable changes in the z-spectra after lysing the blood, highlighted in Fig. 4(d) which directly compares z-spectra from fresh and lysed cRBCs. Whilst the most significant changes in the spectra are due to the changes in relaxation times, the NOE-1.7ppm signal is not apparent in the lysed blood despite the reduction in DS in this region of the spectrum (Fig. 4(d) inset). Fig. 4(e) shows there is little change in the z-spectra on clotting the concentrated RBCs except for a reduction in the NOE-1.7ppm signal (Fig. 4(e) inset).

The LD model fitted the spectra well and the results are shown in Table 4. In the LD fitting we assumed a symmetric MT lineshape as observed in the *ex vivo* blood and sagittal sinus spectra. However, we also attempted to fit an asymmetric MT lineshape but the AREX results were unchanged.

Fig. 5 shows the AREX signals for the NOE-3.5ppm, APT, amine and MT for both the fresh and lysed oxygenated, deoxygenated, control and concentrated RBCs blood samples, for the three saturation powers separately. NOE-1.7 ppm AREX values could not be calculated as they tend to infinity due to their close proximity to the DS peak (Heo et al., 2017). The NOE-3.5ppm, APT, and amine AREX signals showed an average 40% increase between the control sample and concentrated RBCs samples.

The NOE-3.5ppm AREX signal showed a trend to be higher at low B_1

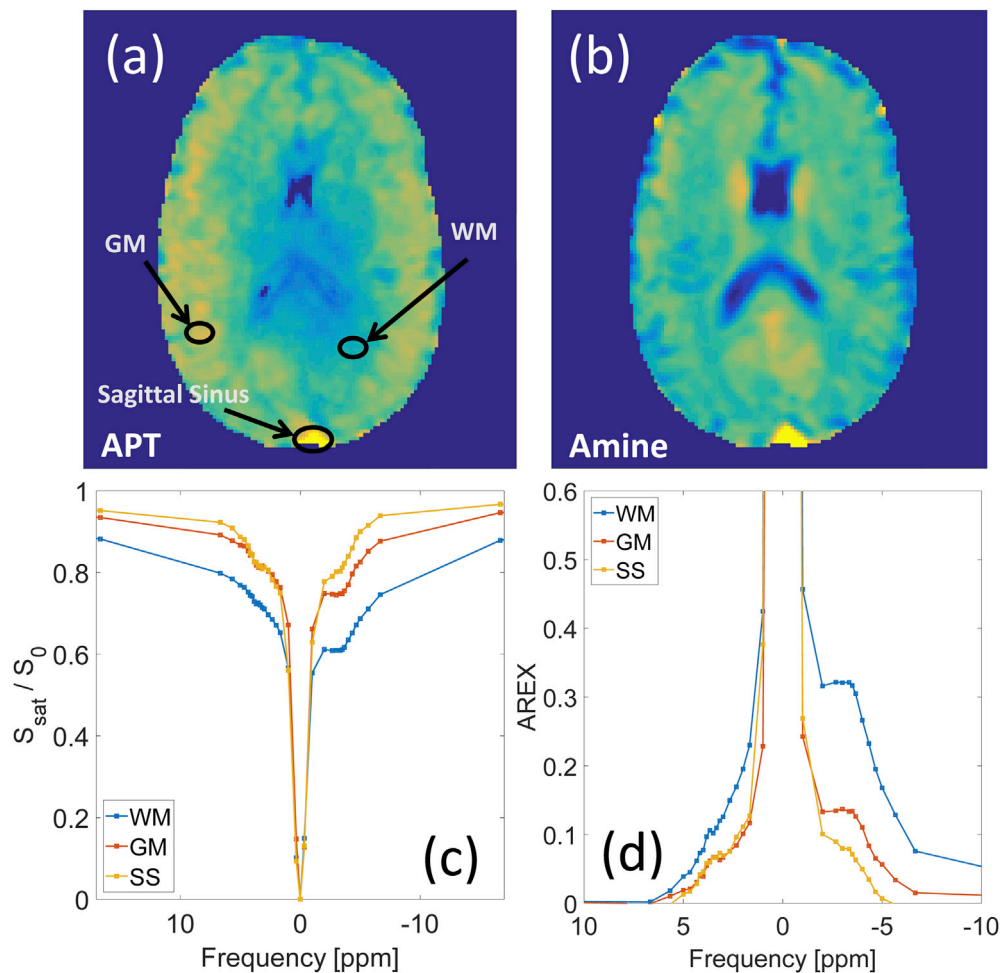


Fig. 2. Lorentzian difference maps (B_1 corrected to a target of 0.5 μT) for (a) APT and (b) amine maps. The corresponding (c) z-spectra (d) AREX spectra (with the MT contribution removed) for the three ROIs indicated on the APT map are also shown.

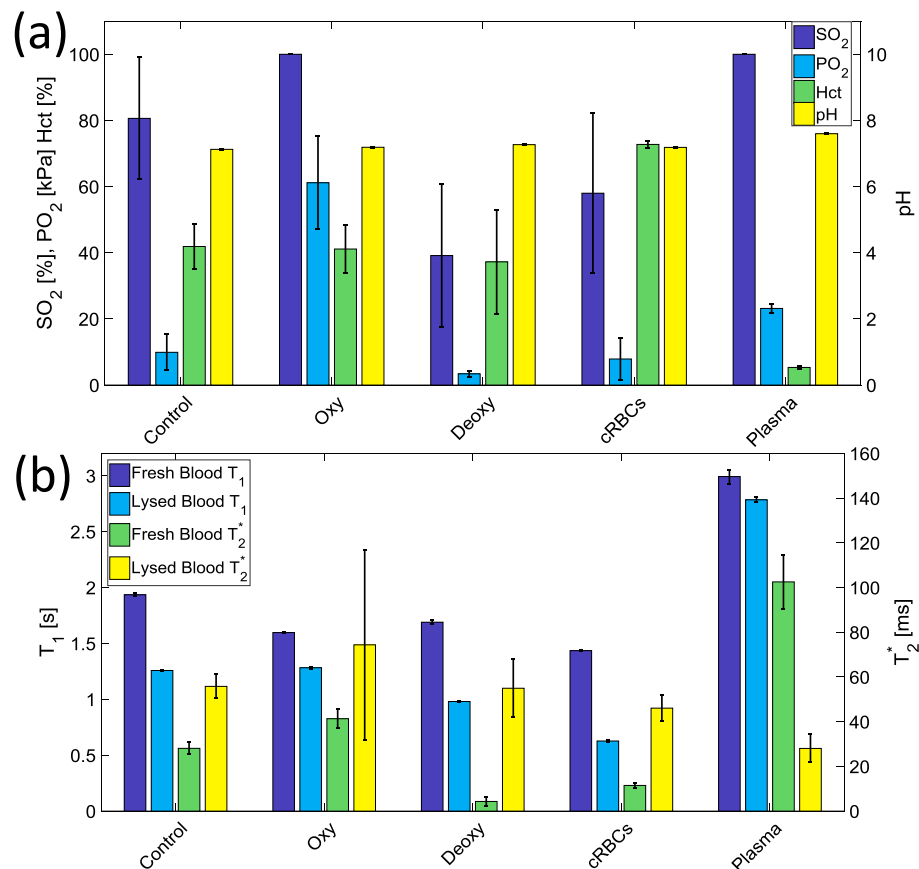


Fig. 3. (a) The saturation of oxygen (SO₂), partial pressure of oxygen (PO₂), pH levels and the haematocrit levels of the control, oxygenated, deoxygenated, concentrated RBCs and plasma blood samples, and (b) the average T₁ and T₂* for fresh and lysed blood samples separately.

power for all samples, whereas the APT, amine and MT pools sizes tended to increase across all B₁ powers, except for the control sample amine AREX signal which dropped at high power, possibly because of its close proximity to the DS peak.

Comparing the control, oxygenated and deoxygenated blood samples for each power with 2 way-ANOVA, the NOE-_{3.5ppm} AREX pool showed no significant change with oxygenation ($p = 0.59$), but upon lysing fell by an average of 27% for all samples ($p = 0.003$). The APT signal also showed no significant change on oxygenation ($p = 0.67$) and fell by an average of 22% ($p = 0.01$) on lysing. There was no significant difference between the fresh and lysed amines ($p = 0.06$). The MT signal fell by an average of 60% on lysing ($p = 0.017$) for the 1.3 μ T saturation (the low power signal was too small to compare).

Fig. 6 shows effects of pH on the z-spectra and AREX signal when the blood was buffered to pH 6.8, 7.0 and 7.4, and suggests that both the NOE-_{3.5ppm} and APT exchanges are base catalysed.

Fig. 7(a) shows the Bloch-McConnell 6-pool model fitted to z-spectra obtained for the fresh and lysed control blood samples as well as for the fresh and lysed concentrated RBCs for three different combination of B₁ saturation powers. Table 5 shows the results of the 16 parameter fit with ranges of fitted values consistent with halving the SNR as an indication of the uncertainty in the fit. The apparent range T₂s of the APT and amine exchanging proton pools in Table 5 are shorter than those previously found in grey matter, whilst the T₂ of the MT is longer.

Fig. 7(b–f) show the results of the final 5 parameter fit to the 6 pool model for the fresh and lysed control and concentrated samples and compares the results to AREX for the mid saturation power (taken from Fig. 5).

Discussion

Significant CEST signals can be detected from major blood vessels on *in vivo* MRI and here we have shown that these signals can also be detected in blood *ex vivo*. Amide and amine (which are related to proteins and amino acids) signals and two NOE peaks were detected in the z-spectrum from blood. The results indicate that these signals originate largely from RBCs and do not depend significantly upon blood oxygenation. Upon lysing the blood we observed a significant decrease in the amide, NOE-_{3.5ppm} and MT AREX signal and the NOE-_{1.7ppm} peak disappeared (inset in Fig. 4(d)). The source of NOE-_{3.5ppm} signal is currently under debate but is assumed to derive from aliphatic and olefinic protons in mobile proteins involving direct dipole-dipole interactions and exchanged relayed interactions (Jones et al., 2013) (in the brain NOE-_{3.5ppm} has been reported to be closely related to myelin (Mougin et al., 2013)).

Any z-spectrum signal from blood is crucial for the interpretation of endogenous z-spectrum signals detected *in vivo*. For example the effect of a change in blood volume must be considered when studying a change in APT signal from a tumour, or the effects of possible blood break down products must be considered when studying a patient with a stroke.

Fig. 4(a) indicates that the z-spectrum features arise largely from the red blood cells rather than the plasma. Signals were observed in the z-spectrum of plasma (Fig. 4(a)) probably related to amines in albumin and other plasma proteins and possibly residual red blood cells, but the longer T₁ of the plasma (Fig. 2(b)) will have accentuated the exchanging peaks. To account for this we calculated the T₁ corrected AREX spectra (Fig. 4(a) inset) and found that the NOE, APT and MT signals were more than 8 times greater in the cRBC samples than the plasma samples.

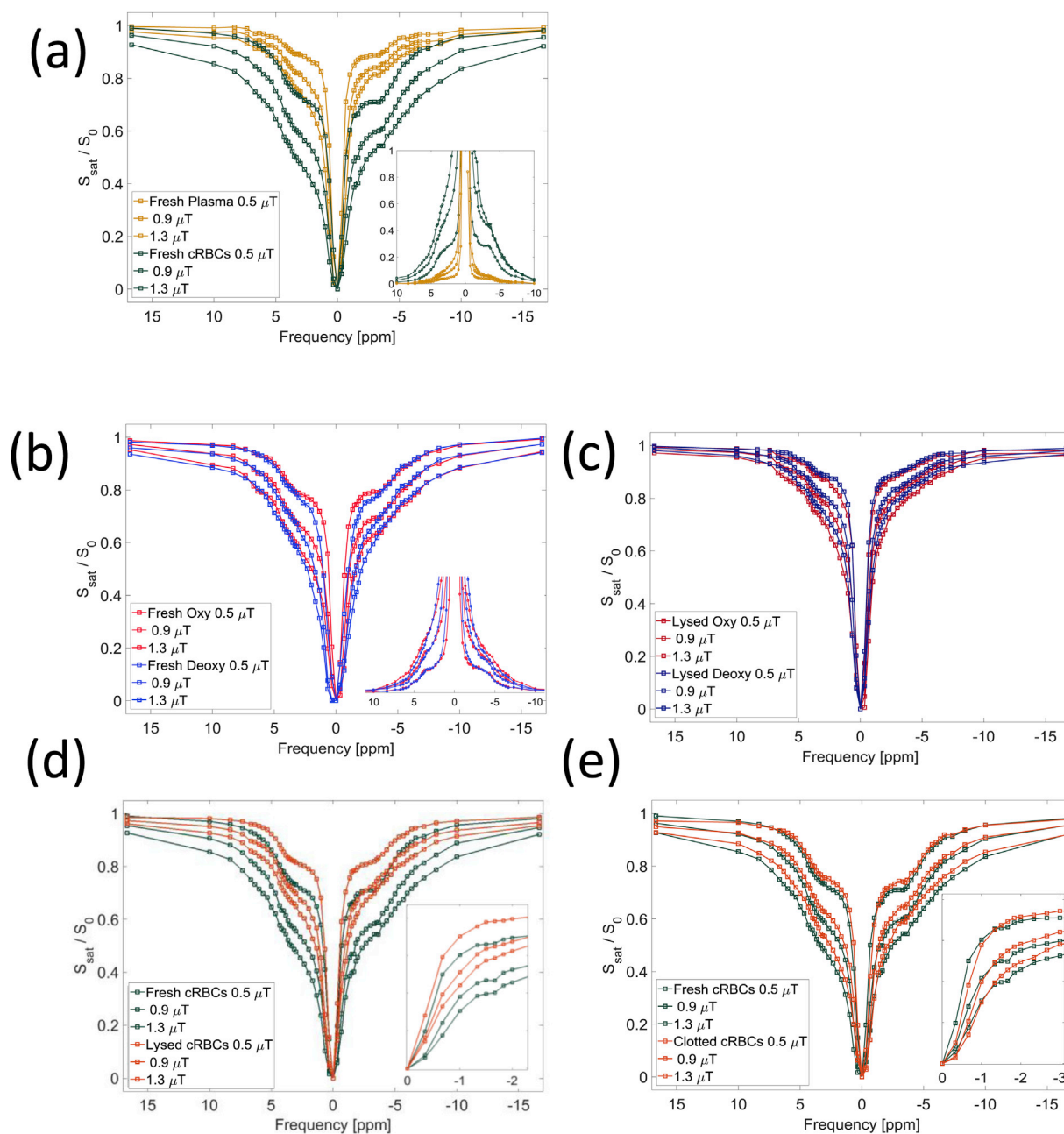


Fig. 4. B_1 corrected z-spectra for the (a) fresh plasma and concentrated RBCs with (inset) the AREX spectra for the fresh cRBCs and plasma, (b) fresh oxygenated and deoxygenated blood with (inset) the AREX spectra for the fresh oxygenated and deoxygenated blood, (c) B_1 corrected z-spectra for the lysed oxygenated and deoxygenated blood with (inset) a zoom in around -1.7 ppm, (d) fresh and lysed concentrated RBCs and (e) fresh and clotted concentrated RBCs with (inset) a zoom in around -1.7 ppm. All are presented at the target B_1 saturation powers of 0.5, 0.9 and 1.3 μT .

Table 4

The peak widths and position for APT, amines, NOEs, DS and MT from the LD model fitting.

	APT	Amines	NOE $_{-1.7\text{ppm}}$	NOE $_{-3.5\text{ppm}}$	DS	MT
Fitted peak position averaged over all samples (ppm)	3.55 ± 0.04	2.08 ± 0.02	Fixed at -1.7 ppm	-3.49 ± 0.01	0.02 ± 0.02	0.43 ± 0.19
Fitted peak width for oxygenated samples (ppm)	3.5 ± 0.3	1.90 ± 0.09	0.52 ± 0.05	4.7 ± 0.2	1.62 ± 0.04	36.8 ± 4.2
Fitted peak width for deoxygenate-d samples (ppm)	3.2 ± 0.1	2.90 ± 0.02	1.3 ± 0.2	4.4 ± 0.2	2.17 ± 0.07	40.0 ± 1.9

There was an increase in all z-spectrum features in the concentrated red blood cell sample (Fig. 4(a) and (b)), and the AREX which gives a relative signal for NOE $_{-3.5\text{ppm}}$ and APT, showed there was an average 40% increase between the control, oxygenated or deoxygenated samples and, the concentrated RBCs samples, which corresponds to the measured increase in haematocrit (42%). Similar results were obtained for the BM fit

except for NOE $_{-3.5\text{ppm}}$ which was underestimated for lysed cRBCs. The pH was measured before and after scanning, and a drop in pH of 0.2–0.3 for all the blood samples was detected which would have modified the results since exchange rates of amides (and amines to a lesser extent) are base catalysed (Zhou et al., 2003).

Deoxygenated haemoglobin is highly paramagnetic and oxygenated

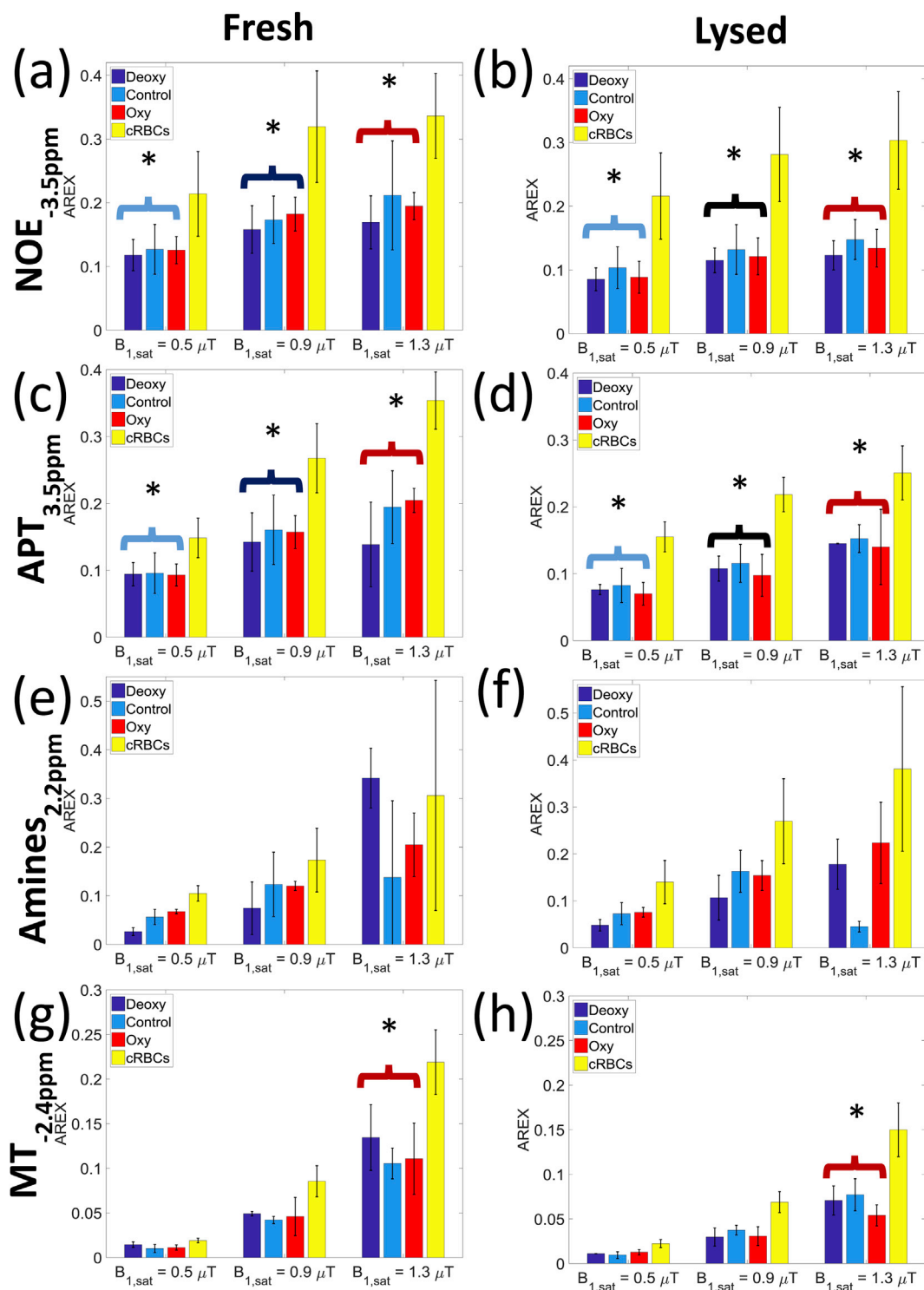


Fig. 5. The calculated AREX from the Lorentzian lineshape fitting, showing the NOE_{-3.5ppm}, APT_{3.5ppm} and Amine_{2.2ppm} and MT_{-2.4ppm} signals for the deoxygenated, control, oxygenated and cRBCs blood samples for the target saturation powers 0.5, 0.9 and 1.3 μ T. Statistical (2 way ANOVA) tests showed that were significant differences between the fresh and lysed blood samples, across the saturation powers.

haemoglobin is slightly diamagnetic relative to plasma, whilst dissolved oxygen makes plasma paramagnetic. In deoxygenated blood this results in magnetic field gradients around the red blood cells leading to the observed shorter T_2^* and broader DS peak (Weisskoff and Kiihne, 1992). The net frequency of the sample will also have been shifted by 0.48 ppm up-field (Gasparovic and Matwiyoff, 1992), but we only considered relative frequency shifts. A small negative variation of T_1 with oxygenation might have been expected (d'Othée et al., 2003; Blockley et al.,

2008) but in fact the control blood had the longest T_1 . This was probably because the oxygenated samples all had an SO_2 of 100% causing oxygen to be dissolved in the plasma reducing T_1 (Ma et al., 2016). The T_1 of (not oxygenated) plasma was similar to CSF. The main observable difference between the z-spectra of oxygenated and deoxygenated blood (Fig. 4(b)) was the narrower DS peak consistent with the fact that the samples had similar T_1 s and very different T_2^* s. However, the results of the AREX fitting, was performed separately at each power, do suggest some trends

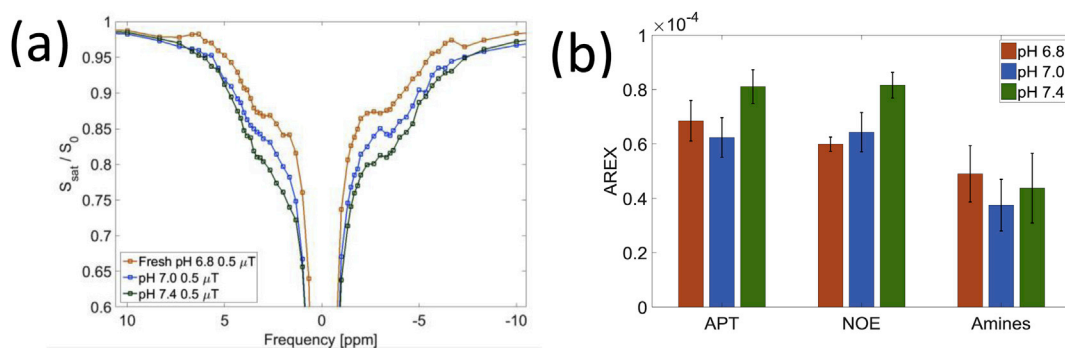


Fig. 6. (a) Z-spectra for blood with pH 6.8, 7.0 and 7.4 showing an effect on the APT and $NOE_{-3.5ppm}$ signal change at B_1 corrected target saturation power of 0.5 μ T (b) AREX for the APT, $NOE_{-3.5ppm}$ and Amines at a target power of 0.5 μ T respectively for the blood with pH 6.8, 7.0 and 7.4.

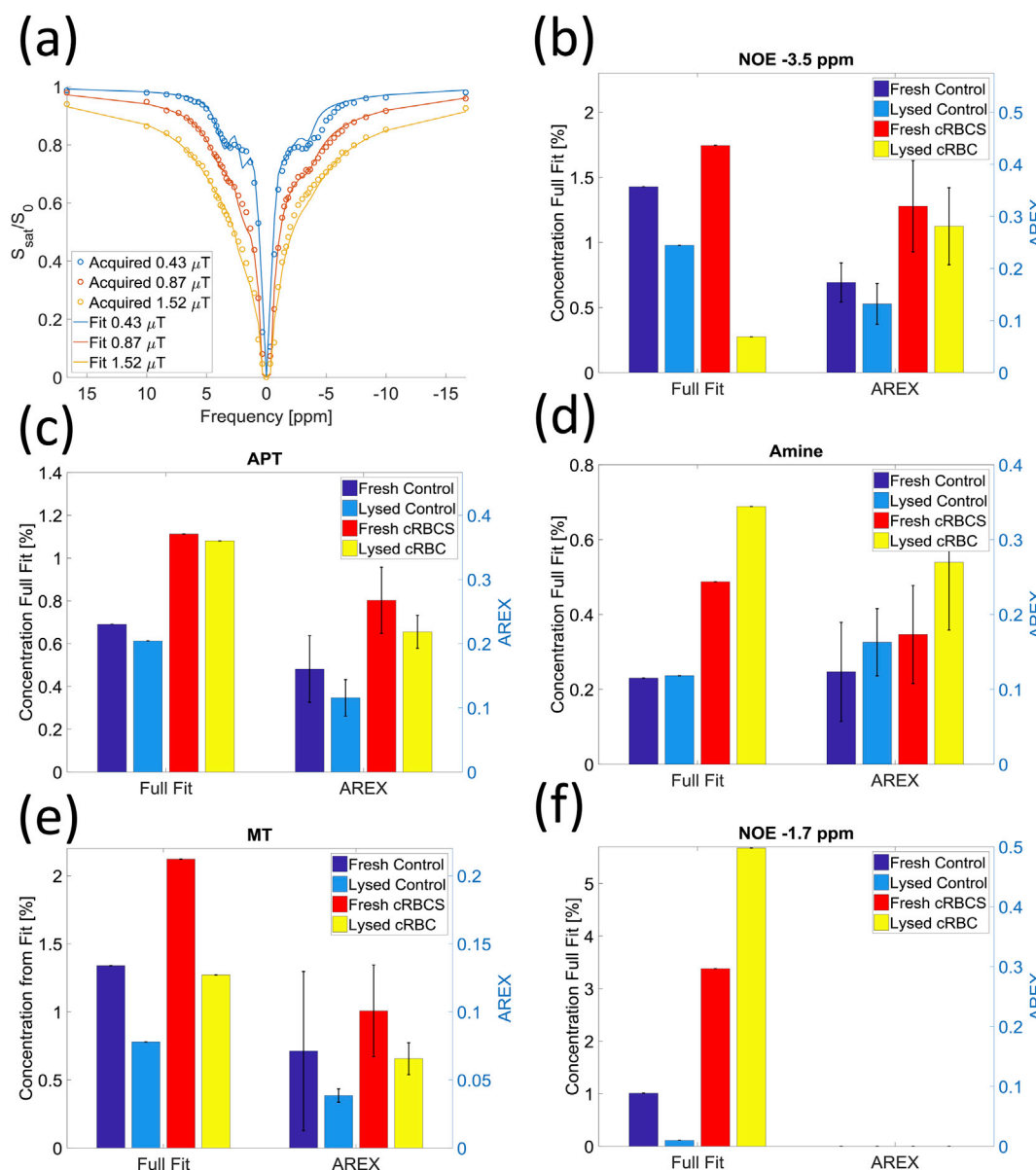


Fig. 7. (a) 16 parameters fitted using the 6 pool Bloch McConnell equations on the control fresh blood sample. The fit results are presented in Table 5 (b–f) Estimated pool size of $NOE_{-3.5ppm}$, APT, Amines MT and $NOE_{-1.7ppm}$ from the final 5 parameter Bloch McConnell fit. vs. the AREX results for the target B_1 saturation of 0.9 μ T are also shown. The AREX signal cannot be calculate for $NOE_{-1.7ppm}$.

for the amine signal to increase with oxygenation, possibly related to the change in conformation of the haemoglobin molecule (which contains

histadine) on oxidation (the results at high power are less reliable due to the effects of DS on the AREX calculation close to resonance).

Table 5

Results of the 16 parameter fit to the 6 pool Bloch-McConnell fitting of the z-spectra acquired on the control blood samples, together with an indication of the uncertainty in the fit.

	APT	Amines	NOE -1.7ppm	NOE -3.5ppm	MT
Pool concentration (%)	0.78	0.39	1.80	1.44	1.05
	0.78–1.29	0.01–0.64	0.58–2.80	0.44–2.47	0.36–1.30
Exchange rate (Hz)	33.1	338.7	6.35	4.9	10.3
	6.3–50.0	120–481	5.3–15.6	2.9–10	10.3–27.8
T_2 (ms)	1.4	30.7	1.5	5.9	0.093
	1.4–6.5	13.6–58.7	1.5–8.4	1.4–9.0	0.023–0.093

After lysing, T_2^* increased for all blood samples, which is expected because of the homogenization of the sample. T_1 decreased particularly for the deoxygenated sample which may be related to the fact that lysing can lead to the formation of methaemoglobin which has a particularly high T_1 relaxivity. After lysing the DS peak was narrowed and the MT baseline, CEST and NOE features reduced in amplitude which would be consistent with the known effects assuming an increase in T_2^* and a reduction in the T_1 . Both AREX and the BM analysis attempt to correct for the effects of such changes in T_1 , and indicated a significant reduction in NOE $_{-3.5\text{ppm}}$, APT and MT on lysing. The reduction in MT, APT and NOE $_{-3.5\text{ppm}}$ upon lysing suggests that these are related to the semi-solid intracellular and membrane components which are denatured as the RBCs are destroyed. The AREX NOE $_{-3.5\text{ppm}}$ in the plasma (Fig. 4(a)) is likely to be associated with albumin but was measured to be 7 times less than the AREX NOE $_{-3.5\text{ppm}}$ in the lysed cRBCs (results not shown). Lysing is associated with both conversion of haemoglobin to methaemoglobin and changes in the cell membrane, but the trend for the NOE $_{-3.5\text{ppm}}$ AREX signal to be reduced particularly for the oxygenated blood, might point to this effect originating in haemoglobin.

Clotting had surprisingly little effect on the z-spectrum. However both lysing and clotting caused the NOE $_{-1.7\text{ppm}}$ peak to disappear. This could not be quantified by AREX since the NOE $_{-1.7\text{ppm}}$ peak was so close to the DS peak. Similarly the BM fit did not properly fit the NOE $_{-1.7\text{ppm}}$ for the cRBCs, probably due to its sensitivity to the estimate of T_2 . AREX quantification of amines has only been successfully employed at 9.4T (Zhang et al., 2017b). Examining all the z-spectra the NOE $_{-1.7\text{ppm}}$ signal is visible in the unclotted, unlysed blood, and particularly in cRBCs, and at low pH. This could be related to a result recently reported by Zhang et al. who examined an 'NOE mediated MT effect around -1.6ppm ' and observed a strong contrast difference between healthy and stroke tissue in rats (Zhang et al., 2016). Future work will focus on determining this frequency more precisely. At increased ionic strength (or osmolarity) red blood cells can form echinocytes (or burr cells) losing their discoid shape and gaining small protrusions on their surface, associated with separation of the lipid bilayer from the underlying membrane skeleton (Liu et al., 1989), and similar effects are observed *in vivo* in various situations where the cells are under stress. Previous work using ^1H NMR suggests that echinocyte formation is associated with changes in the distribution of phospholipids between the two leaflets of the cell membrane (Pages et al., 2010). It has recently been shown that reconstituted egg phospholipids show an NOE $_{-1.7\text{ppm}}$ peak (Zhang et al., 2017a). It seems possible that morphological transformation of the cell membrane is in some way responsible for the change in the NOE $_{-1.7\text{ppm}}$ peak although further work including optical microscopy is required to confirm this.

The increase in the amine signal estimated by AREX with B_1 is consistent with amines being in faster exchange than the other pools and thus requiring more B_1 saturation power to observe magnetisation exchange of the protons of interest. The discrepancy for the control sample at high power is due to the broad DS peak which perturbed the LD model fit for that sample. There is good agreement between AREX at medium power and the BM model as shown in Fig. 7.

In this work the data were analysed quantitatively in two ways: by fitting to an LD model with AREX analysis which yields a relative CEST or NOE proton signal but does not measure the pool sizes, and by fitting to a

BM model which gives absolute proton pool sizes (relative to the water pool) and an estimate of T_{i2} , and $k_{i,\text{ex}}$ for the exchanging pools. Fig. 7 shows generally good agreement between the relative pool sizes estimated from the two methods. However only relative quantification is possible with AREX. For instance for LD fitting, spline interpolation was used to correct for B_1 field inhomogeneities at 7T (Windschuh et al., 2015; Jones et al., 2011), but the AREX results clearly varied with B_1 saturation power in a way that depended on exchange rate (Jones et al., 2011). AREX is also unable to cope with coalescing peaks, particularly close to the water peak. Furthermore the AREX theory was derived for a spin system in a steady state (Jones et al., 2011), which may not be achieved for samples with longer T_1 using a finite train of saturation pulses. Simulations of the pre-saturation pulse trains used in our experiments (40 pulses in 2.4 s) showed the system achieved approximately 95% of steady state at the end of the pulse train. The full BM fit does not require the system to reach steady state. The BM fit was performed on a subset of the samples which allowed us to test whether it was possible to detect changes expected due to changes in concentration, but it was still compromised for NOE $_{-1.7\text{ppm}}$ probably due to errors in the estimate of T_2 which are likely to have also affected the fit to the amine peak. The exchange rates and relaxation times measured in the control blood sample from the BM fit were generally of the same order of magnitude as the values measured in the brain (van Zijl et al., 2017). The T_2 values were somewhat shorter than previously reported, despite the fact that the blood was less structured than brain tissue. This may indicate that the peaks identified actually correspond to multiple peaks which have not been accounted for in the BM model. The exchange rates measured for amines suggest that they may originate more in guanidinium (which can be found in creatine and the arginine side groups in proteins) at 2 ppm rather than glutamate at 3 ppm (van Zijl et al., 2017) since the guanidinium proton group has a lower exchange rate than amine protons (Chen et al., 2017). In general the relaxation times measured were shorter which might be expected given the reduced structure in blood compared to grey matter. These values can provide starting values for future investigations of blood and possible multicompartmental modelling of tissue. Future work will use continuous wave saturation to provide improved spectra and will fit a range of samples to explore the effects of blood oxygenation and pH on T_{i2} , and $k_{i,\text{ex}}$.

Conclusion

This work has shown that the CEST and NOE effects seen in z-spectra of *ex vivo* blood originate primarily from the RBCs and that the z-spectrum from blood shows a diverse range of CEST and NOE effects, some of which depend on whether or not the cells have been lysed. These results are crucial to our interpretation of *in vivo* z-spectra in pathology, where changes in blood volume need to be considered.

Acknowledgements

This work was supported by the Medical Research Council [grant number MR/M009122/1]; and carried out using the facilities of the Sir Peter Mansfield Imaging Centre (SPMIC). The Centre's facilities have also been funded by EPSRC, HEFCE, Wellcome and the University of Nottingham.

References

- Blockley, N.P., Jiang, L., Gardener, A.G., Ludman, C.N., Francis, S.T., Gowland, P.A., Dec 2008. Field strength dependence of R1 and R2* relaxivities of human whole blood to ProHance, Vasovist, and deoxyhemoglobin. *Magn. Reson. Med.* 60, 1313–1320.
- Cai, K., Haris, M., Singh, A., Kogan, F., Greenberg, J.H., Hariharan, H., et al., 2012. Magnetic resonance imaging of glutamate. *Nat. Med.* 18, 302–306, 2012/01/22.
- Cai, K.J., Singh, A., Poptani, H., Li, W.G., Yang, S.L., Lu, Y., et al., Jan 2015. CEST signal at 2ppm (CEST@2ppm) from Z-spectral fitting correlates with creatine distribution in brain tumor. *Nmr Biomed.* 28, 1–8.
- Chappell, M.A., Donahue, M.J., Tee, Y.K., Khrapitchev, A.A., Sibson, N.R., Jezzard, P., et al., Aug 2013. Quantitative Bayesian model-based analysis of amide proton transfer MRI. *Magn. Reson. Med.* 70, 556–567.
- Chen, L., Zeng, H., Xu, X., Yadav, N.N., Cai, S., Puts, N.A., et al., Sep 29 2017. Investigation of the contribution of total creatine to the CEST Z-spectrum of brain using a knockout mouse model. *NMR Biomed.* (in press).
- d'Othée, B.J., Rachmuth, G., Munasinghe, J., Lang, E.V., 2003. The effect of hyperoxygenation on T1 relaxation time in vitro. *Acad. Radiol.* 10, 854–860.
- Gardener, A.G., Francis, S.T., Prior, M., Peters, A., Gowland, P.A., 2010. Dependence of blood R2 relaxivity on CPMG echo-spacing at 2.35 and 7 T. *Magnetic Reson. Med.* 64, 967–974.
- Gasparovic, C., Matwyoff, N.A., Aug 1992. The magnetic-properties and water dynamics of the red-blood-cell - a study by proton-Nmr lineshape analysis. *Magnetic Reson. Med.* 26, 274–299.
- Geades, N., Hunt, B.A., Shah, S.M., Peters, A., Mougin, O.E., Gowland, P.A., 2017. Quantitative analysis of the z-spectrum using a numerically simulated look-up table: application to the healthy human brain at 7T. *Magn. Reson. Med.* 78 (2), 645–655.
- Haris, M., Singh, A., Cai, K., Kogan, F., McGarvey, J., DeBrosse, C., et al., 2014. A technique for in vivo mapping of myocardial creatine kinase metabolism. *Nat. Med.* 20, 209–214, 2014/01/12.
- Heo, H.Y., Lee, D.H., Zhang, Y., Zhao, X., Jiang, S., Chen, M., Zhou, J., 2017. Insight into the quantitative metrics of chemical exchange saturation transfer (CEST) imaging. *Magn. Reson. Med.* 77 (5), 1853–1865.
- Hua, J., Jones, C.K., Blakeley, J., Smith, S.A., van Zijl, P.C., Zhou, J., Oct 2007. Quantitative description of the asymmetry in magnetization transfer effects around the water resonance in the human brain. *Magn. Reson. Med.* 58, 786–793.
- Jones, C.K., Polders, D., Hua, J., Zhu, H., Hoogduin, H.J., Zhou, J., et al., 2011. In vivo three-dimensional whole-brain pulsed steady-state chemical exchange saturation transfer at 7 T. *Magnetic Reson. Med.* 67, 1579–1589, 2011/11/14.
- Jones, C.K., Huang, A., Xu, J., Edden, R.A., Schär, M., Hua, J., et al., 2013. Nuclear Overhauser enhancement (NOE) imaging in the human brain at 7T. *Neuroimage* 77, 114–124.
- Liu, S.C., Derick, L.H., Duquette, M.A., Palek, J., Aug 1989. Separation of the lipid bilayer from the membrane skeleton during discocyte-echinocyte transformation of human erythrocyte ghosts. *Eur. J. Cell Biol.* 49, 358–365.
- Liu, G.S., Song, X.L., Chan, K.W.Y., McMahon, M.T., Jul 2013. Nuts and bolts of chemical exchange saturation transfer MRI. *Nmr Biomed.* 26, 810–828.
- Ma, Y., Berman, A.J., Pike, G.B., Dec 2016. The effect of dissolved oxygen on the relaxation rates of blood plasma: implications for hyperoxia calibrated BOLD. *Magn. Reson. Med.* 76, 1905–1911.
- McVicar, N., Li, A.X., Goncalves, D.F., Bellyou, M., Meakin, S.O., Prado, M.A.M., et al., Apr 2014. Quantitative tissue pH measurement during cerebral ischemia using amine and amide concentration-independent detection (AACID) with MRI. *J. Cereb. Blood Flow Metabolism* 34, 690–698.
- Morrison, C., Henkelman, R.M., Apr 1995. A model for magnetization transfer in tissues. *Magn. Reson. Med.* 33, 475–482.
- Mougin, O., Clemence, M., Peters, A., Pitiot, A., Gowland, P., Nov 2013. High-resolution imaging of magnetisation transfer and nuclear Overhauser effect in the human visual cortex at 7 T. *Nmr Biomed.* 26, 1508–1517.
- Pages, G., Yau, T.W., Kuchel, P.W., Sep 2010. Erythrocyte shape reversion from echinocytes to discocytes: kinetics via fast-measurement NMR diffusion-diffraction. *Magn. Reson. Med.* 64, 645–652.
- Rivlin, M., Horev, J., Tsarfaty, I., Navon, G., Oct 25 2013. Scientific Reports. Molecular Imaging of Tumors and Metastases Using Chemical Exchange Saturation Transfer (CEST) MRI, vol. 3.
- van Zijl, P.C., Yadav, N.N., Apr 2011. Chemical exchange saturation transfer (CEST): what is in a name and what isn't? *Magn. Reson. Med.* 65, 927–948.
- van Zijl, P.C., Jones, C.K., Ren, J., Malloy, C.R., Sherry, A.D., Mar 13 2007. MRI detection of glycogen in vivo by using chemical exchange saturation transfer imaging (glycoCEST). *Proc. Natl. Acad. Sci. U. S. A.* 104, 4359–4364.
- van Zijl, P.C.M., Lam, W.W., Xu, J., Knutsson, L., Stanisz, G.J., Apr 21 2017. Magnetization transfer contrast and chemical exchange saturation transfer MRI. Features and analysis of the field-dependent saturation spectrum. *Neuroimage*. <https://doi.org/10.1016/j.neuroimage.2017.04.045> (in press).
- Walker-Samuel, S., Ramasawmy, R., Torrealdea, F., Rega, M., Rajkumar, V., Johnson, S.P., et al., Aug 2013. In vivo imaging of glucose uptake and metabolism in tumors. *Nat. Med.* 19, 1067.
- Ward, K.M., Aletras, A.H., Balaban, R.S., Mar 2000. A new class of contrast agents for MRI based on proton chemical exchange dependent saturation transfer (CEST). *J. Magn. Reson.* 143, 79–87.
- Weisskoff, R.M., Kiihne, S., Apr 1992. MRI susceptometry: image-based measurement of absolute susceptibility of MR contrast agents and human blood. *Magn. Reson. Med.* 24, 375–383.
- Windschuh, J., Zaiss, M., Meissner, J.E., Paech, D., Radbruch, A., Ladd, M.E., et al., May 2015. Correction of B1-inhomogeneities for relaxation-compensated CEST imaging at 7T. *Nmr Biomed.* 28, 529–537.
- Woessner, D.E., Zhang, S., Merritt, M.E., Sherry, A.D., 2005. Numerical solution of the Bloch equations provides insights into the optimum design of PARACEST agents for MRI. *Magnetic Reson. Med.* 53, 790–799.
- Xu, X., Yadav, N.N., Zeng, H., Jones, C.K., Zhou, J., van Zijl, P.C., et al., Jan 2016. Magnetization transfer contrast-suppressed imaging of amide proton transfer and relayed nuclear overhauser enhancement chemical exchange saturation transfer effects in the human brain at 7T. *Magn. Reson. Med.* 75, 88–96.
- Yan, K., Fu, Z., Yang, C., Zhang, K., Jiang, S., Lee, D.-H., et al., 2015. Assessing amide proton transfer (APT) MRI contrast origins in 9 L gliosarcoma in the rat brain using proteomic analysis. *Mol. Imaging Biol.* 17, 479–487.
- Yarnykh, V.L., Jan 2007. Actual flip-angle imaging in the pulsed steady state: a method for rapid three-dimensional mapping of the transmitted radiofrequency field. *Magn. Reson. Med.* 57, 192–200.
- Zaiss, M., Bachert, P., Nov 21 2013. Chemical exchange saturation transfer (CEST) and MR Z-spectroscopy in vivo: a review of theoretical approaches and methods. *Phys. Med. Biol.* 58, R221–R269.
- Zaiss, M., Schmitt, B., Bachert, P., Aug 2011. Quantitative separation of CEST effect from magnetization transfer and spillover effects by Lorentzian-line-fit analysis of z-spectra. *J. Magn. Reson.* 211, 149–155.
- Zaiss, M., Windschuh, J., Paech, D., Meissner, J.E., Burth, S., Schmitt, B., et al., May 15 2015. Relaxation-compensated CEST-MRI of the human brain at 7 T: Unbiased insight into NOE and amide signal changes in human glioblastoma. *Neuroimage* 112, 180–188.
- Zhang, X.Y., Wang, F., Afzal, A., Xu, J., Gore, J.C., Gochberg, D.F., et al., Oct 2016. A new NOE-mediated MT signal at around -1.6ppm for detecting ischemic stroke in rat brain. *Magn. Reson. Imaging* 34, 1100–1106.
- Zhang, X.Y., Wang, F., Jin, T., Xu, J., Xie, J., Gochberg, D.F., et al., Aug 2017. MR imaging of a novel NOE-mediated magnetization transfer with water in rat brain at 9.4 T. *Magn. Reson. Med.* 78, 588–597.
- Zhang, X.Y., Wang, F., Li, H., Xu, J., Gochberg, D.F., Gore, J.C., et al., July 2017b. CEST imaging of fast exchanging amine pools with corrections for competing effects at 9.4 T. *NMR Biomed.* 30 (7).
- Zheng, S., van der Bom, I.M., Zu, Z., Lin, G., Zhao, Y., Gounis, M.J., 2014. Chemical exchange saturation transfer effect in blood. *Magnetic Reson. Med.* 71, 1082–1092.
- Zhou, J.Y., van Zijl, P.C.M., May 30 2006. Chemical exchange saturation transfer imaging and spectroscopy. *Prog. Nucl. Magnetic Reson. Spectrosc.* 48, 109–136.
- Zhou, J., Payen, J.-F., Wilson, D.A., Traystman, R.J., van Zijl, P.C.M., 2003. Using the amide proton signals of intracellular proteins and peptides to detect pH effects in MRI. *Nat. Med.* 9, 1085–1090, 2003/07/20.
- Zhou, J., Wilson, D.A., Sun, P.Z., Klaus, J.A., Van Zijl, P.C., May 2004. Quantitative description of proton exchange processes between water and endogenous and exogenous agents for WEX, CEST, and APT experiments. *Magn. Reson. Med.* 51, 945–952.